Cellular and Molecular Bioengineering (© 2018)
https://doi.org/10.1007/s12195-018-0525-z

Graphene Microelectrode Arrays for Electrical and Optical Measurements of Human Stem Cell-Derived Cardiomyocytes

SAHIL KUMAR RASTOGI,[1] JACQUELINE BLILEY,[1] DANIEL J. SHIWARSKI,[1] GURUPRASAD RAGHAVAN,[3] ADAM W. FEINBERG,[1,2] and TZAHI COHEN-KARNI [1,2]

[1]Department of Biomedical Engineering, Carnegie Mellon University, Pittsburgh, PA 15213, USA; [2]Department of Materials Science and Engineering, Carnegie Mellon University, Pittsburgh, PA 15213, USA; and [3]Division of Biology and Biological Engineering, California Institute of Technology, Pasadena, CA 91125, USA

(Received 19 February 2018; accepted 26 April 2018)

Associate Editor William E. Bentley oversaw the review of this article.

Abstract—*Introduction*—Cell–cell communication plays a pivotal role in biological systems' coordination and function. Electrical properties have been linked to specification and differentiation of stem cells into targeted progeny, such as neurons and cardiomyocytes. Currently, there is a critical need in developing new ways to complement fluorescent indicators, such as Ca^{2+}-sensitive dyes, for direct electrophysiological measurements of cells and tissue. Here, we report a unique transparent and biocompatible graphene-based electrical platform that enables electrical and optical investigation of human embryonic stem cell-derived cardiomyocytes' (hESC-CMs) intracellular processes and intercellular communication.
Methods—Graphene, a honeycomb sp^2 hybridized two-dimensional carbon lattice, was synthesized using low pressure chemical vapor deposition system, and was tested for biocompatibility. Au and graphene microelectrode arrays (MEAs) were fabricated using well-established microfabrication methods. Au and graphene MEAs were interfaced with hESC-CMs to perform both optical and electrical recordings.
Results—Optical imaging and Raman spectroscopy confirmed the presence of monolayer graphene. Viability assay showed biocompatibility of graphene. Electrochemical characterization proved graphene's functional activity. Nitric acid treatment further enhanced the electrochemical properties of graphene. Graphene electrodes' transparency enabled both optical and electrical recordings from hESC-CMs. Graphene MEA detected changes in beating frequency and field potential duration upon β-adrenergic receptor agonist treatment.
Conclusion—The transparent graphene platform enables the investigation of both intracellular and intercellular communication processes and will create new avenues for bidirectional communication (sensing and stimulation) with electrically active tissues and will set the ground for investigations reported diseases such as Alzheimer, Parkinson's disease and arrhythmias.

Keywords—Transparent electrodes, Calcium imaging, High spatial and temporal resolution, Bioelectronics, hESC-CM, Graphene.

Address correspondence to Tzahi Cohen-Karni, Department of Biomedical Engineering, Carnegie Mellon University, Pittsburgh, PA 15213, USA. Electronic mail: tzahi@andrew.cmu.edu

Tzahi Cohen-Karni is an assistant professor at the departments of Biomedical Engineering and Materials Science and Engineering in Carnegie Mellon University, Pittsburgh PA USA. He received both his B.Sc. degree in Materials Engineering and the B.A. degree in Chemistry from the Technion Israel Institute of Technology, Haifa, Israel, in 2004. His M.Sc. degree in Chemistry from Weizmann Institute of Science, Rehovot, Israel, in 2006 and his Ph.D. in Applied Physics from the School of Engineering and Applied Sciences, Harvard University, Cambridge MA, USA, in 2011. He was a Juvenile Diabetes Research Foundation (JDRF) Postdoctoral Fellow at the Massachusetts Institute of Technology and Boston Children's Hospital at the labs of Robert Langer and Daniel S. Kohane from 2011 to 2013. Dr. Cohen-Karni received the Gold Graduate Student Award from the Materials Research Society in 2009, and received the 2012 International Union of Pure and Applied Chemistry Young Chemist Award. In 2014, he was awarded the Charles E. Kaufman Foundation Young Investigator Research Award. In 2016, Dr. Cohen-Karni was awarded the NSF CAREER Award. In 2017, Dr. Cohen-Karni was awarded the Cellular and Molecular Bioengineering Rising Star Award, The Office of Naval Research Young Investigator Award and The George Tallman Ladd Research Award.

This article is part of the 2018 CMBE Young Innovators special issue.

Published online: 04 May 2018

INTRODUCTION

Cell–cell communication plays a pivotal role in biological systems' coordination and function. Electrical properties have recently been linked to specification and differentiation of stem cells into targeted progeny such as neurons and cardiomyocytes.[3,30,44] Basic research at the tissue level of the heart and brain electrical activity has led to the development of tools to treat various ailments, such as pacemaker and deep brain stimulation electrodes.[9,12] Human embryonic stem cells (hESCs) and induced pluripotent stem cells (hiPSCs)-derived cardiomyocytes (CMs) provide a promising tool to study cardiac developmental biology, regenerative therapies, disease modeling, and drug discovery.[20,23,33,36,46] These cells represent human-like physiology and have the potential to self-renew indefinitely thus are advantageous over the traditional cells and *ex vivo* models obtained from animals.[23,46] Electrophysiology is a powerful tool to study the maturity of CMs, their functional properties, effect of therapeutics on cellular physiology, and intercellular communication.[5,22,33]

Studies of electroactive cells such as hESC-CMs have been carried out using a variety of techniques, including glass micropipette patch-clamp electrodes,[5] voltage and Ca^{2+} sensitive dyes,[18] and microelectrode arrays (MEAs).[5,7,22,32] Patch clamp technique enables electrical recording at a single cell level with high temporal resolution, however it is limited to only a few cells at a time, making it ineffective to monitor activity of large cellular networks.[43] MEA uses established microfabrication methods to allow multiplexed detection on a scale not possible with micropipette technology. However, it exhibits relatively large detection areas that render both cellular and subcellular electrical recording immensely challenging.[43] Complementing electrical recording with optical imaging using fluorescent indicators such as Ca^{2+} sensitive dyes[18] can leverage the temporal resolution and spatial advantages of both the techniques. Commonly used metal-based MEAs have high opacity which hinders simultaneous optical and electrical recordings. Previously, indium tin oxide (ITO)[16] and bilayer nanomesh[39]-based electrodes have been developed as transparent platforms, however, they are either limited by the brittle nature of the electrode material or limited transparency over a wide spectral range. Therefore, developing a platform that allows simultaneous electrical recordings and optical measurements over a wide visible spectral range will enable measurements at high spatial and temporal resolution, and will potentially enable optical stimulation of the cells at electrode-cell interface using optogenetics.[10]

Since the discovery of graphene,[35] a honey-combed arrangement of sp^2 hybridized carbon atoms, there has been an immense interest in its use for bio-interfaces, due to its outstanding electrical conductivity (charge carrier mobility up to 200,000 $cm^2\ V^{-1}\ s^{-1}$), mechanical flexibility, high transparency of up to 97.7%, and biocompatibility.[8,15,24,26,37,40] Here, we report a graphene-based transparent and biocompatible platform to perform simultaneous Ca^{2+} imaging and electrical recordings in hESC-CMs as illustrated in Fig. 1. First, monolayer graphene was synthesized using low pressure chemical vapor deposition (LPCVD) and transferred to a glass coverslip or a Si/285 nm SiO_2 substrate (Fig. 1a). Second, the samples were annealed under reducing environment to enhance adhesion between graphene sheet and the substrate. Third, the devices were fabricated by patterning graphene sheet into electrodes with 50 μm × 50 μm recording sites, followed by patterning and evaporating Au interconnects, and a polymer (SU8) passivation layer (Fig. 1b). For control, Au MEAs were fabricated with the same design and dimensions as the graphene MEAs. Prior to passivation, graphene electrodes were treated with 69% w/w HNO_3 acid for 2 h to enhance graphene's electrochemical properties. Fourth, the surfaces of the devices were coated with fibronectin, and the fibronectin-conditioned hESC-CMs were seeded on the devices. Finally, simultaneous electrical and optical recordings were obtained from the spontaneously beating CMs (Fig. 1c).

MATERIALS AND METHODS

Graphene Synthesis and Transfer

A single layer of graphene was synthesized by a Cu-catalyzed low pressure chemical vapor deposition (LPCVD) process as previously described.[31,40] Briefly, a 2 cm × 6 cm Cu foil (99.8%, Alfa Aesar, uncoated, catalog no. 46365) was cleaned with acetone and isopropyl alcohol (IPA) in an ultrasonic bath for 5 min each then N_2 blow dried. Before being introduced into a custom-built CVD setup, the foil was treated with a 5.4% w/w HNO_3 solution (CMOS Grade, J.T. Baker, catalog no. JT9606-3) for 30 s, rinsed three times with deionized (DI) water and N_2 blow dried. The synthesis process was carried out at 1050 °C and a total pressure of 0.5 Torr. The temperature was ramped up to 1050 °C in 20 min, followed by stabilization at 1050 °C for 5 min under the flow of 100 standard cubic centimeters per minute (sccm) Ar. The foil was annealed for 60 min under H_2 flow of 100 sccm, followed by a synthesis step of 8 min under the flow of 50 sccm CH_4 (5% in Ar, Matheson Gas) and 100 sccm H_2

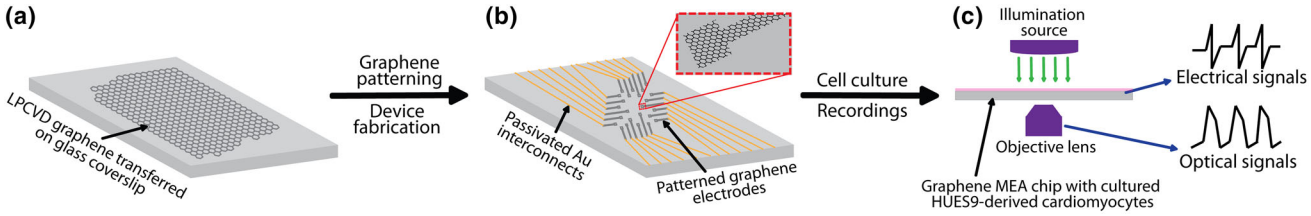

FIGURE 1. Schematics of graphene microelectrode array (MEA) fabrication and recording. (a) Low pressure chemical vapor deposition (LPCVD) synthesized monolayer graphene transferred on glass coverslip. (b) Fabricated graphene MEA. (c) Simultaneous optical and electrical recordings from human embryonic stem cells-derived cardiomyocytes (HUES9-CMs) cultured on graphene MEA.

(Matheson Gas). The sample was rapidly cooled from growth temperature down to 100 °C in 30 min while flowing 100 sccm Ar. The Cu foil with graphene on both sides was cut into the required dimensions. Prior to Cu etching one side of the foil was coated with 200 nm of polymethylmethacrylate (PMMA 950 A4 MicroChem) to mechanically support the graphene and protect it from the subsequent steps. The foil was placed in a UV-ozone cleaner (PSD Pro series digital UV-Ozone, Novascan) and the graphene on the uncoated side was etched for 15 min at 100 °C. The Cu foil was wet-etched in a solution containing 25% w/w $FeCl_3.6H_2O$ (Sigma Aldrich, catalog no. 31232), 4% w/w HCl acid (CMOS grade, J.T. Baker, catalog no. BDH3028) and 71% w/w DI water. At the end of the etching process the PMMA supported graphene film was transferred to clean DI water three times. Depending on the subsequent experimental requirements, the resulting water floating graphene was transferred either to a glass coverslip (VWR, catalog no. 48366-227), quartz substrate (76.2 mm ST-cut single crystal quartz wafer, University Wafer) or (100) Si substrate with a 285 nm wet thermal oxide (p-type, 0.001–0.005 Ω cm, Nova Electronic Materials Ltd., catalog no. CP02-11208). Prior to the graphene transfer, the substrates were cleaned with acetone in an ultrasonic bath for 5 min followed by IPA wash and N_2 blow dry. The transferred samples were air-dried overnight. The substrates were then baked at 150 °C for 30 min, followed by dissolving the PMMA in an acetone bath at 60 °C for 30 min. Finally, the samples were rinsed with acetone and IPA and N_2 blow dried.

Graphene Characterization

Transmittance of graphene was characterized using a UV–vis spectrophotometer (Shimadzu UV-2600). The spectra were obtained for graphene film transferred on a 2 cm × 2 cm quartz substrate. Bare 2 cm × 2 cm quartz substrates were used as a reference material.

Raman spectroscopy of graphene film was performed by NT-MDT NTEGRA Spectra (100X/0.7 NA objective) under 532 nm excitation. For the Raman spectra a laser power of 2.3 mW was used, and the spectra were recorded with an acquisition time of 30–60 s.

Device Fabrication

LPCVD synthesized graphene was transferred to 22 mm × 22 mm glass coverslips or 18 mm × 18 mm Si/285 nm SiO_2 chips. The samples were annealed at ambient pressure in a reducing environment under 10 sccm H_2 flow for 1 h at 300 °C. Graphene was patterned using photolithography and reactive ion etching techniques. Briefly, 300 nm LOR3A (MicroChem) and 500 nm Shipley S1805 (MicroChem) were coated on substrates with graphene sheet; the resist was patterned by UV exposure using a mask aligner (Karl Suss MA6) followed by development for 1 min in CD26 developer (MicroChem); graphene from the un-patterned regions was etched off by reactive ion etching (Plasma Therm 790 RIE) using 14 sccm O_2 and 6 sccm Ar at 20 W power and 10 mTorr pressure for 1 min. Post etching, the LOR3A/Shipley stack was stripped off using Remover PG (MicroChem). The Au interconnects and contacts were then patterned using similar photolithography technique, and 5 nm Cr (99.99%, R.D. Mathis Co.) and 100 nm Au (99.999%, Praxair) were deposited using thermal evaporator (Angstrom Engineering Covap II). For Au MEA control, graphene electrode region was replaced with Cr/Au (5/100 nm) electrodes, and for no graphene MEA control, neither graphene nor Au was present in the recording site region. For graphene electrodes, 69% w/w HNO_3 acid treatment was performed for 2 h followed by three times DI water rinses. Finally, the Au interconnects and the non-recording site of the graphene electrodes were passivated with 200 nm of SU-8 2000.5 (MicroChem) using photolithography.

Electrochemical Characterization

CV experiments were performed in a three-electrode cell setup using a potentiostat (PalmSens 3). Elec-

trolyte solution of 1 M KCl (≥ 99%, Sigma-Aldrich, catalog no. P5405) was prepared in DI water. Analyte solution of 5 mM ferrocene methanol (FcMeOH) (97%, Sigma-Aldrich, Catalog No. 335061) was prepared in 1 M KCl solution. Prior to conducting CV experiments, a polystyrene well was sealed to the sample using 10:1 base:curing agent poly dimethylsiloxane (PDMS) (Sylgard 184 Silicone Elastomer, Dow Corning). Pt wire and Ag/AgCl electrodes were used for counter and reference electrodes, respectively. To determine the faradaic peaks, the CV measurements were recorded within a potential range from − 0.2 to 0.6 V vs. Ag/AgCl at scan rates of 80–500 mV s^{-1} in the presence of 5 mM FcMeOH in 1 M KCl solution. For capacitive currents, CV was conducted with 1 M KCl electrolyte solution within a potential range from − 0.2 to 0.3 V vs. Ag/AgCl at scan rates of 100–800 mV s^{-1}.

EIS experiments were performed in a three-electrode cell setup using a potentiostat (CH Instruments, CHI660C). 1X Phosphate Buffered Saline (PBS) (ThermoFisher, catalog no. 10010023) was used as an electrolyte solution. Pt wire and Ag/AgCl electrodes were used for counter and reference electrodes, respectively. The frequency was scanned from 0.01 to 100,000 Hz with V_{DC} of 0 V and V_{AC} of 10 mV.

Both CV and EIS experiments were performed on ten electrodes of each of the three independently fabricated chips for each device type (n = 30). The measurements were done inside a grounded aluminum box.

Embryonic Stem Cell Culture and CM Differentiation

Human CMs were differentiated from HUES9 hESCs using established protocols. The HUES9 hESCs were expanded in Essential 8 (E8) medium (Life Technologies, catalog no. A1517001)[6] on 12 $\mu g/cm^2$ geltrex (Life Technologies, catalog no. A1413301)-coated six well plates with an initial seeding density of 125,000 cells/well and passaged every 4 days to prevent over-confluence. For CM differentiation, HUES9 were seeded at a density of 16,000 cells/cm^2 in E8 medium with 2 μM ROCK inhibitor, thiazovivin (Selleck Chemicals, catalog no. S1459) and media was changed daily. On the third day post seeding HUES9 were differentiated into CMs *via* previously described protocols.[6,29] Briefly, cells were washed with 1X PBS and incubated with RPMI-1640 medium (ThermoFisher, catalog no. 21870076) supplemented with B27 minus insulin (ThermoFisher, catalog no. A1895601) and 1% v/v L-glutamine (ThermoFisher, catalog no. 25030081) plus 6 μM CHIR99021 (LC laboratories, catalog no. C-6556), a glycogen synthase kinase-3 inhibitor (LC laboratories, catalog no. S1459) for 2 days. On day 2 of differentiation, cells were washed again with 1X PBS and incubated with RPMI/B27 media and 2 μM Wnt-C59, a Wnt pathway inhibitor (Selleck Chemicals, catalog no. S7037). On day 4 and 6 of differentiation, media was changed with RPMI/B27 media. On day 8 and 10, media was changed to CDM3 media[6] consisting of RPMI-1640 medium supplemented with 1% v/v L-glutamine, 500 μg/mL human albumin (Sigma, catalog no. A9731), and 213 μg/mL L-Ascorbic acid 2-phosphate sesquimagnesium salt hydrate > 95% (Sigma, catalog no. A8960). On day 12, spontaneously beating cells were passaged for CM purification. CMs were purified using lactate-supplemented media, which previous studies have demonstrated achieves 95-98% purification of CMs.[4,47] Briefly, beating CMs were washed with 1X PBS and detached from the surface with TrypLE express (ThermoFisher, catalog no. 12604013) for 15 min at 37 °C. Detached cells were pipetted into DMEM/F12 (ThermoFisher, catalog no. 11320033) and centrifuged at 200 g for 7 min to pellet the cells. CMs were seeded on Matrigel (Corning, catalog no. 356231)-coated plates (12 $\mu g/cm^2$) with RPMI-1640 lacking glucose (ThermoFisher, catalog no. 11879020) and supplemented with 500 μg/mL human albumin, 213 μg/mL L-ascorbic acid-2-phosphate, and 7.1 mM sodium-lactate (Sigma, catalog no. L4263). CMs were purified for 5 days and then switched back to CDM3 for at least 2 days prior to passaging for fibronectin conditioning.

Fibronectin Conditioning of CMs

Prior to seeding CMs onto fibronectin-coated devices, CMs were conditioned on an isotropic coating of fibronectin (Corning, catalog no. 356008) to select for those cells with the ability to bind fibronectin. To create substrates for fibronectin conditioning, six well plates were coated with 1 mL of 50 μg/mL fibronectin per well in sterile distilled water for 1 h at room temperature. Excess fibronectin was then washed with 1X PBS and plates were either used immediately or stored at 4 °C in 1X PBS for less than 2 weeks prior to use. To passage for fibronectin conditioning, CMs were washed with 1X PBS and then lifted with TrypLE for 15 min at 37 °C. Detached cells were pipetted into DMEM/F12 (ThermoFisher, catalog no. 11320033) and centrifuged at 200 g for 7 min to pellet the cells. CMs were then resuspended in CDM3 supplemented with 10% fetal bovine serum (FBS) and 2 μM thiazovivin and seeded onto fibronectin-coated six well plates at a ratio of 1:1.

Biocompatibility Analysis

Cell viability was tested using Live/Dead assay kit (ThermoFisher, catalog no. L3224) containing Calcein

acetoxymethyl (Calcein AM) and Ethidium homodimer dyes for staining live and dead cells, respectively. 1 cm × 1 cm glass and graphene substrates were placed in a 24 well plate and were sterilized with 70% ethanol treatment and 2 h UV exposure in the culture hood. Post sterilization, the chips were rinsed 3 times with 1X PBS, followed by 200 μL of 50 μg/mL fibronectin treatment for 3 h at room temperature. Post incubation the excess fibronectin was pipetted out followed by 3 times 1X PBS wash. The CMs were then seeded at a density of 400,000 cells/cm^2, in a 1 mL CDM3 media supplemented with 10% FBS and 2 μM thiazovivin. The samples were incubated at 37 °C and 5% CO_2 for 10 days with CDM3 media changed every other day. After 10 days, Hoechst 33342 (ThermoFisher, catalog no. 62249), Calcein AM and Ethidium homodimer dyes were added with a final concentration of 1 μg/mL, 2 and 4 μM, respectively, to each sample and incubated for 30 min at 37 °C and 5% CO_2. Cells were then treated with 10 μM Blebbistatin (Sigma Aldrich, catalog no. B0560) to decouple excitation and contraction leading to inhibition of spontaneous cell beating.[25] The cells were washed 3 times with 1X PBS and the live-cell imaging was performed at 37 °C using upright confocal microscope (Nikon A1R) under 20X/0.50 NA water immersion objective.

% Viability quantification[40] was evaluated by:

$$\%\text{Viability} = \frac{\text{Total cells(blue)} - \text{Dead cells(red)}}{\text{Total cells (blue)}} \times 100,$$

where, blue refers to the cells stained by DAPI and red refers to the dead cells stained by Ethidium homodimer. Total cell count was determined by counting the DAPI stained nuclei across five randomly chosen images for each repetition ($n = 3$), using the Fiji particles analysis plugin.

Immunostaining of CMs

Immunostaining of cells was done following established protocols.[14] Briefly, cell culture media was discarded, and the cells were washed with 1X PBS. For fixation and permeabilization, cells were incubated with 4% paraformaldehyde (Electron Microscopy Sciences, catalog no. 15710) and 0.5% Triton-X 100 (Sigma Aldrich, catalog no. X100) for 15 min at room temperature. Cells were washed 3 times with 1X PBS for 5 min each and were incubated with 5% blocking goat serum (ThermoFisher, catalog no. 16210072) for 30 min, followed by 1X PBS wash, and incubation with 0.5% anti-alpha actinin antibody (Sigma Aldrich, catalog no. A7811) for 1 h at room temperature. Cells were washed 3 times with 1X PBS for 5 min each, and were treated with secondary antibody, goat anti-mouse 555 (ThermoFisher, catalog no. A21422) for 1 h, followed by 3 times 1X PBS wash for 5 min each. For nucleus and actin cytoskeleton staining, cells were incubated with 0.5% DAPI (ThermoFisher, catalog no. D1306) and 1.5% Alexa Fluor phalloidin 488 (ThermoFisher, catalog no. A12379), respectively, for 15 min, followed by 3 times 1X PBS wash. The cells were imaged using upright confocal microscope (Nikon A1R) under 20X/0.50 NA water immersion objective.

Electrical and Optical Recordings

Each chip was glued to a printed circuit board (PCB) with soldered 36 pin connector (Omnetics, A79024-001), and all the electrodes on the chip were wire bonded to the Cu pads on the PCB using a manual wedge wire bonder (West Bond 7476D). A 3D printed PLA based frustum chamber was glued to the center of the chip using PDMS for cell culture. Prior to cell seeding, the chips were sterilized with 70% ethanol and 2 h UV exposure in the culture hood. Post sterilization, the chips were rinsed 3 times with 1X PBS, followed by 200 μL of 50 μg/mL fibronectin treatment for 3 h at room temperature. Post incubation, the excess fibronectin was pipetted out followed by 3 times 1X PBS wash. The CMs were then seeded at a density of 400,000 cells/cm^2. The chips were incubated at 37 °C and 5% CO_2 for 7 days. The cell media was changed every other day with a fresh CDM3 media.

At the day of recording, the media in the frustum chamber of each device was discarded and 10 μM Fluo-4 AM (ThermoFisher, catalog no. F14217) prepared in 1X PBS was added to the chamber and incubated at 37 °C for 30 min. Post incubation, the cells were washed 3 times with 1X PBS. PBS was then replaced with Tyrode buffer solution (Sigma-Aldrich, Catalog no. T2145) pre-warmed at 37 °C. The chip was loaded on to the microscope stage, and the temperature inside the culture chamber was maintained by constant perfusion of Tyrode solution maintained at 37 °C using an inline heater (Automate Scientific, Thermoclamp). For electrical recordings, the Omnetics connector on the PCB was connected to a 32-channel amplifier (Intan tech., RHD2132), and the electrical signals were recorded using the Intan acquisition system (Intan tech., RHD2000) at an acquisition rate of 20 kHz. The optical recordings were performed either using an upright confocal microscope (Nikon A1R) under 20X/0.50 NA water immersion objective or an inverted microscope (Nikon TiE) by using a 488 nm excitation laser/light source. All the recordings were performed in a grounded Faraday cage.

Drug Assays

The effects of β-adrenergic receptor agonist, isoproterenol, followed a previously published protocol.[17] Briefly, 10 μM isoproterenol (Sigma-Aldrich, catalog no. I5627) was prepared in Tyrode buffer solution. The drug was perfused to the chamber, and the temperature was maintained at 37 °C by constant flow of drug through the inline heater. Electrical and optical measurements were performed during the drug flow. During drug washout, the drug line was clamped, and fresh Tyrode solution was perfused through the chamber.

Electrical and Optical Data Analysis

The raw data acquired using the Intan acquisition system were analyzed using custom-made MATLAB scripts. The 60 Hz noise was filtered using MATLAB's built-in Butterworth notch filter. The beat frequency was calculated using the Fast Fourier Transform (FFT) function. The findpeaks function was used to detect the Na^+ peaks, and the field potential amplitude (FPA) was calculated by adding the heights of positive and negative peaks. To measure field potential duration (FPD), Na^+ and K^+ peaks were detected using findpeaks function, and the distance between the peaks was calculated. Prior to using findpeaks function, the voltage vs. time curves were smoothened using Savitzky-Golay filtering or sgolayfilt function, to avoid interference of the baseline noise while detecting K^+ peaks. To measure the signal-to-noise ratio (SNR), FPA was divided by the peak-to-peak amplitude of the baseline noise. The peak-to-peak amplitude of the baseline noise was calculated as 6.6 times the standard deviation of the baseline signal.[42]

For calcium signal analysis, the time-lapse image sequences were imported in the Fiji software. A region of interest was selected using the ROI tool and the intensity values were extracted from all the frames using time series analyzer V3 plugin. Corresponding time points were determined using the frame rate of the image acquisition, and the fluorescence intensity vs. time was plotted.

Statistical Analysis

Data are represented as the mean ± standard deviation. Statistical analysis was performed using Student's *t* test (two-tailed) to determine significant difference between two independent groups with one variable i.e. substrates (Fig. S4) and two-way ANOVA followed by Tukey's *post hoc* test for more than two groups with two independent variables: different substrates and drug treatment (Fig. S8). (**) and NS denote statistically significant difference with $p < 0.005$ and no statistically significant difference, respectively.

RESULTS AND DISCUSSION

Graphene Characterization

To characterize graphene film continuity and integrity, LPCVD synthesized graphene was transferred to a Si/285 nm SiO_2, which provides optimal optical contrast for graphene imaging.[2] The optical image confirms high continuity of graphene film with minimal micro-tears (Fig. 2a). To further validate the film quality, Raman spectra of graphene were acquired (Fig. S1A). The presence of a sharp G peak at 1590 ± 1 cm^{-1}, a symmetric 2D peak at 2690 ± 3 cm^{-1} with full width at half-maximum (fwhm) of 36 ± 5 cm^{-1}, and no significant D peak at 1364 ± 4 cm^{-1}, indicates presence of defect-free monolayer graphene (Table S1).[41] The 32-electrode Au and graphene MEA devices were fabricated on both glass coverslips and Si/285 nm SiO_2 substrates. Figure 2b shows an optical image of a graphene MEA fabricated on a glass coverslip, demonstrating the transparency of the center region with 32 graphene

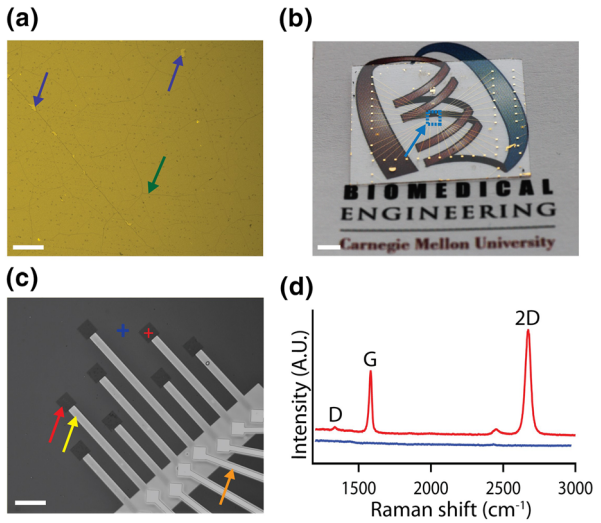

FIGURE 2. Characterization of graphene MEA. (a) DIC image of LPCVD synthesized monolayer graphene transferred on Si/285 nm SiO_2 substrate. Purple and green arrows indicate tears and grain boundary in the graphene film, respectively. Scale bar: 100 μm. (b) Image of a graphene MEA fabricated on a glass coverslip. Cyan arrow marks the area with graphene electrodes (cyan dashed box). Scale bar: 2 mm. (c) DIC image of the graphene MEA fabricated on a Si/285 nm SiO_2 substrate. Red, yellow and orange arrows indicate exposed graphene, SU8 passivated both graphene and Au interconnects, respectively. Scale bar: 100 μm. (d) Raman spectra acquired from graphene electrode and non-electrode regions marked by red and blue crosses, respectively in (c).

electrodes (Cyan dashed box). The presence of monolayer and high transparency of graphene was further confirmed by UV–Vis spectroscopy that shows ca 97.7% transmittance (Fig. S1B).[45] The dip in the transmittance spectra at 250 nm is observed due to the presence of benzene rings in the graphene sheet.[34] The expanded view of the graphene MEA fabricated on a Si/285 nm SiO_2 chip (Fig. 2c) and glass coverslip (Fig. S2), show the patterned passivated graphene electrodes. The Raman spectra (Fig. 2d) confirms the patterning of graphene electrodes with no damage to the film during the fabrication process. The blue shifts in the G and 2D peaks of 8 ± 2 and 4 ± 2 cm^{-1}, respectively, post HNO_3 acid treatment confirms the p-type doping of graphene (Fig. S1C, Table S2).[27,28]

Electrochemical Characterization

For the electrochemical characterization of the electrodes, cyclic voltammetry (CV) and electrode impedance spectroscopy (EIS) were performed in a three-electrode electrochemical cell. To test the functionality of graphene electrodes, CV was performed at varying scan rates and compared to Au electrodes. A conductive electrode enables electrochemical oxidation and reduction of a redox probe or analyte.[1] Absence of graphene electrodes resulted with no current recorded, indicating that the Au interconnects are properly passivated (Fig. 3a). The 50 μm × 50 μm graphene electrodes resolved the reduction and oxidation peaks of FcMeOH similar to that of Au electrodes indicating that graphene is electrochemically active (Figs. 3a and S3A, B).[1] Interfacing electrodes with the electrolyte leads to a formation of an electrical double layer that behaves as a capacitor.[1] Sweeping the potential across the working electrode with respect to the reference electrode leads to the capacitive currents, as observed for both graphene and Au electrodes (Figs. 3B and S3D, E). Treatment of graphene with HNO_3 acid enhanced the faradaic and capacitive currents (Figs. 3a, 3b, and S3C, F) due to the increase in charge carriers and oxide containing species on the surface of graphene leading to pseudo-capacitance.[21,48] These observations were consistent for CV performed at varying scan rates (Fig. S3). To further characterize the impedance of the electrodes EIS was performed. The Au and graphene electrodes show an impedance of 1.2 ± 0.2 and 2.1 ± 0.3 MΩ, respectively, measured at 1 kHz (Fig. 3c). The impedance of the graphene electrodes dropped down to 1.5 ± 0.2 MΩ after HNO_3 acid treatment, which can be explained by the increase in charge carriers due to p-type doping introduced by HNO_3.[21] The phase plots indicate that Au electrodes exhibit more resistive characteristics at high frequencies and more capacitive characteristics at lower frequencies.[26] Graphene electrodes show a deviation in the capacitive properties compared to Au electrodes which might be attributed to quantum capacitance of

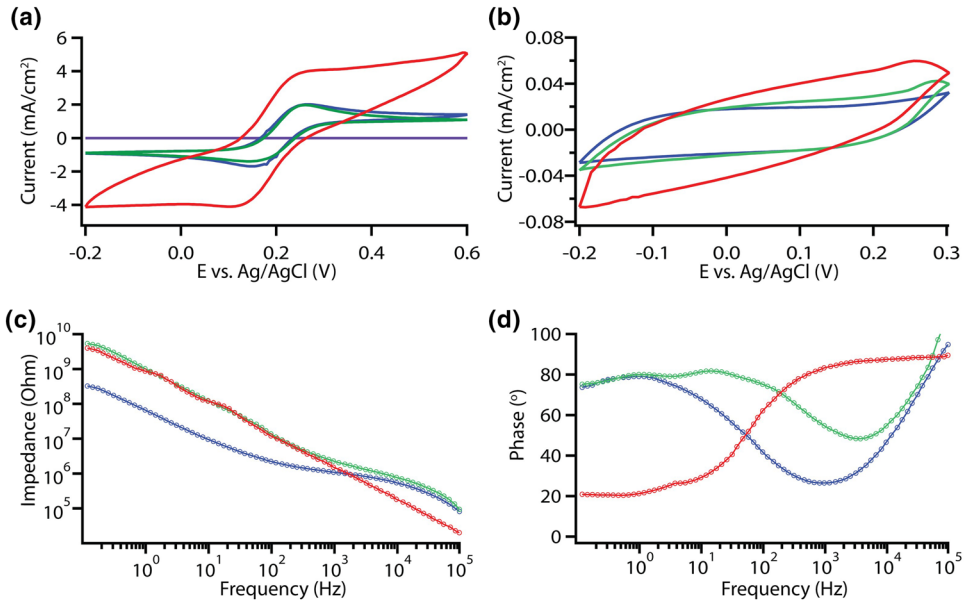

FIGURE 3. Electrochemical characterization of MEAs. (a) Cyclic voltammograms of 50 μm × 50 μm electrodes acquired with 5 mM ferrocene methanol (FcMeOH) in 1 M KCl at 500 mV/s. (b) Cyclic voltammograms acquired with 1 M KCl at 800 mV/s. (c) Impedance vs. frequency plots for 50 μm × 50 μm electrodes. (d) Phase vs. frequency plots for 50 μm × 50 μm electrodes. Purple, green, blue and red traces denote no graphene control, graphene electrode, Au electrode, and HNO_3 treated graphene electrode, respectively.

graphene.[13,49] The HNO_3 acid treatment enhanced the capacitive characteristics of graphene, which is in line with the increase in capacitive currents in the CV curves performed with 1 M KCl (Fig. 3b).

Biocompatibility Analysis

Cellular viability was assessed by a Calcein acetoxymethyl and Ethidium homodimer based Live/Dead assay before interfacing the graphene-based electrodes with the cells.[40] As evident from the fluorescent and DIC images of the hESC-CMs cultured on glass coverslips and graphene substrates for 10 days (Fig. S4A, B), graphene substrates had no detectable cytotoxic effects on cell viability. The cell viability of $> 95\%$ on both control and graphene substrates confirms biocompatibility of graphene (Fig. S4C). These findings are in line with previously published data regarding biocompatibility of graphene interfaced with nonneuronal and neuronal cells.[40]

Simultaneous Electrical and Optical Recordings

The Au and graphene electrodes were then interfaced with hESC-CMs for simultaneous electrical and calcium imaging. The immunofluorescent and DIC images of the cells (Fig. S5) show that the cells spread out uniformly on the MEA chip with graphene electrodes. The immunostaining of alpha-actinin bands confirms the presence of CMs.[33] The low impedance of Au electrodes leads to recording of field potentials at high SNR, however, the high opacity of Au electrodes hinders the visualization of cells at the electrode interface (Figs. 4a(I) and S6A). The Au electrodes recorded the field potentials with spike frequency of ca. 1.4 Hz at high SNR of ca. 17 (Fig. 4a(II)). The high temporal resolution of electrical recordings provides information about the Na^+ current (upstroke), K^+ current (repolarization) and Ca^{2+} current (plateau phase) across the cell membrane with recorded field potential amplitude (FPA) of 880 ± 15 μV and field potential duration (FPD) of 214 ± 10 ms ($n = 87$

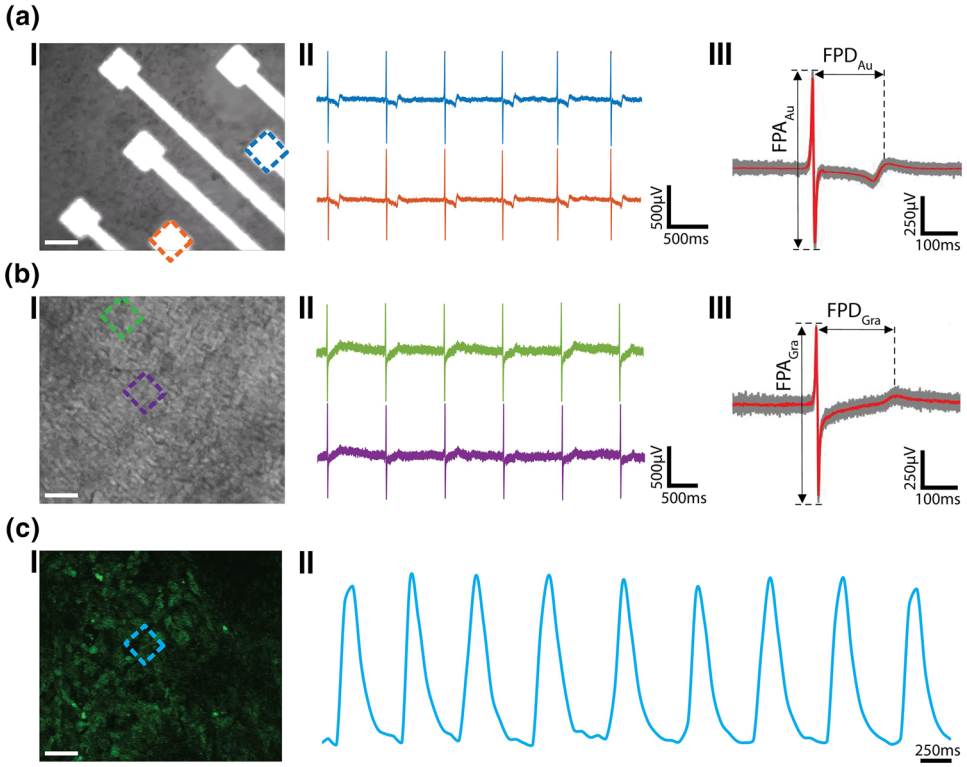

FIGURE 4. Electrical and optical signals recordings. (a) Electrical recordings using Au MEA. (I) Optical image of HUES9-CMs cultured on Au MEA. Scale bar: 50 μm. (II) Representative recorded field potential traces using Au electrodes marked in (I). (III) Averaged peak (red trace) and raw data (grey traces, 87 peaks). (b) Electrical recordings using graphene MEA. (I) Optical image of HUES9-CMs cultured on graphene MEA. Scale bar: 50 μm. (II) Representative recorded field potential traces using graphene electrodes marked in (I). (III) Averaged peak (red trace) and raw data (grey traces, 70 peaks). FPA and FPD denote field potential amplitude and field potential duration, respectively. (c) Calcium fluorescence signal recordings. (I) Confocal image of HUES9-CMs loaded with Fluo-4 dye, cultured on graphene electrodes. Scale bar: 50 μm. (II) Fluorescence intensity as function of time at the electrode region marked in (I).

peaks) (Fig. 4a(III)).[32] The graphene electrodes, on the other hand, allowed the visualization of the cells at the electrode interface owing to the high transparency of electrodes (Figs. 4b(I) and S6B). The graphene electrodes also enabled recording of field potentials with high SNR of ca. 14, spike frequency of ca. 1.1 Hz, and FPA of 815 ± 12 μV and FPD of 217 ± 9 ms (n = 70 peaks) (Fig. 4b(II, III)). The values for beating frequency, FPD and FPA are in line with the previously reported values.[5,23,32] The high transparency of graphene electrodes also enabled simultaneous Ca^{2+} imaging (Figs. 4c(I) and S7A, Video S1). The Ca^{2+} spike frequency extracted from the time lapse imaging of Ca^{2+} sensitive dye (Fluo-4) labeled cells matches the electrical spike frequency recorded using the electrodes. This shows the ease of performing simultaneous recordings, thus allowing integration of the advantages of both modes of recording, leading to high spatial and temporal resolution.

Drug Assays

To further validate the recorded electrical signals and check if graphene MEA platform can be used to detect changes in electrophysiology, the cells were treated with a standard drug, isoproterenol that stimulates the β-adrenergic receptors leading to an increase in beat frequency and a decrease in FPD.[17] Figures 5a(I) and 5b(I) show 1.3 fold increase in the peak frequency from 1.4 to 1.8 Hz in case of Au electrodes, and 1.2 fold increase from 1.1 to 1.3 Hz in case of graphene electrodes. The increase in the beat frequency was further supported by the simultaneous Ca^{2+} imaging performed on the cells interfaced with graphene electrodes (Fig. S7B, Video S2). The addition of the drug led to 0.9 fold decrease in FPD from 215 ± 9 to 187 ± 3 ms for Au electrodes (n = 350 peaks across 5 channels) (Figs. 5a(II) and S8), and 0.9 fold decrease from 215 ± 7 to 195 ± 6 ms for graphene electrodes (n = 350 peaks across 5 channels) (Figs. 5b(II) and S8). The beat frequency returned to its original value post washout of isoproterenol (Fig. S9), suggesting feasibility of performing multiple assays on the same electrode-cell setup.

CONCLUSION

In conclusion, we demonstrated that the graphene electrodes enable simultaneous electrical and optical recordings from hESC-CMs without affecting either of the recording modes. The high temporal resolution of the electrical recording provides information about all three ionic currents involved in action potential (i.e., Na^+, K^+ and Ca^{2+}), whereas high spatial resolution of the Ca^{2+} imaging provides information at a single

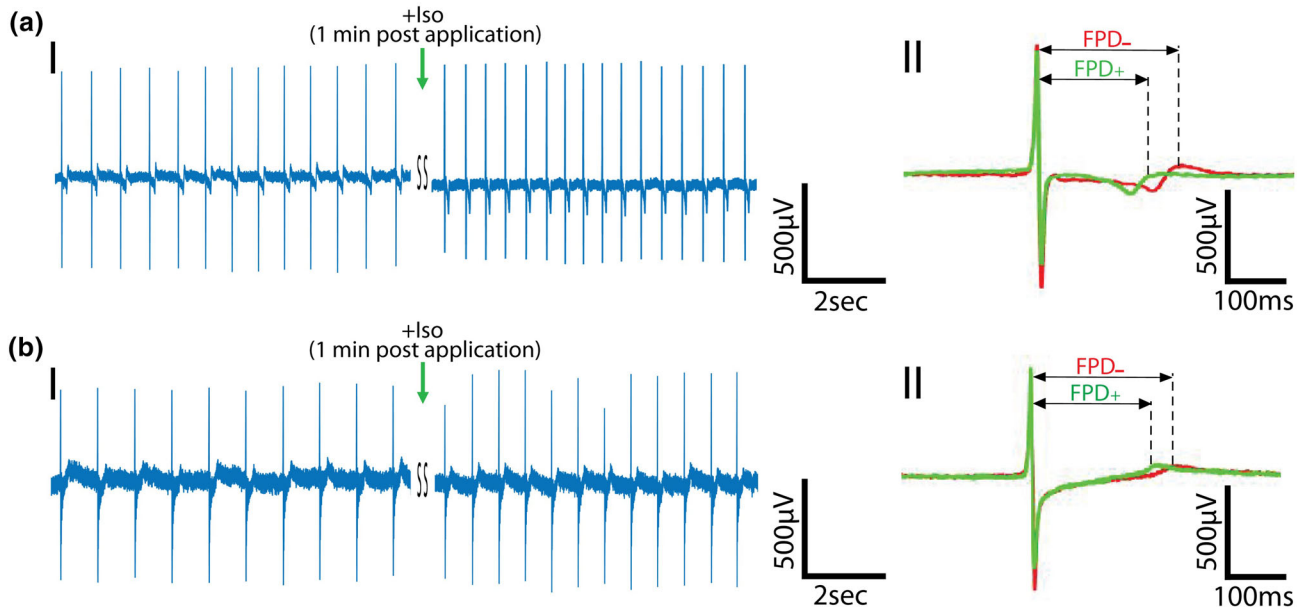

FIGURE 5. Effect of β-adrenergic receptor agonist on the recorded electrical signals. (a) Representative recorded field potential trace using Au MEA. (I) Recorded trace before and after application of the β-adrenergic receptor agonist, isoproterenol. (II) Averaged trace (87 peaks) before (red, −) and after (green, +) isoproterenol application. (b) Representative recorded field potential trace using graphene MEA. (I) Recorded trace before and after application of the β-adrenergic receptor agonist, isoproterenol. (II) Averaged trace (70 peaks) before (red, −) and after (green, +) isoproterenol application. Green arrow represents the addition of drug.

cell level. The HNO_3 acid treatment of graphene led to electrode impedance reduction to values similar to Au electrodes, thus enabling recording of electrical signals at high SNR of ca. 14. This further indicates the flexibility and ease of surface modification of graphene electrodes to enhance their electrochemical properties. The fabrication protocol suggested in this work can be easily extended to dense arrays of graphene electrodes to enable recording and studying of larger cellular networks. The biocompatibility of graphene demonstrated in this work and previous studies[40] indicates the potential of graphene-based devices for long term stable tissue interfaces. The major advantage of the presented platform is the high transparency of the electrodes, which provides the flexibility to perform simultaneous optical studies for both electrophysiology applications such as Ca^{2+} imaging, and non-electrophysiology applications such as optogenetic manipulation of the cells,[10] optical coherence tomography (OCT) imaging,[37] monitoring biochemical activity of the cells using fluorescently labeled dyes and proteins,[11,19,38] and further investigation of the tissue health[40] at the electrode-cell interface over time. The developed nanomaterials-based measurement platform will set the ground for further investigations of the relationship between electrical signals and reported diseases such as Alzheimer, Parkinson's disease and arrhythmias.

ELECTRONIC SUPPLEMENTARY MATERIAL

The online version of this article (https://doi.org/10.1007/s12195-018-0525-z) contains supplementary material, which is available to authorized users.

ACKNOWLEDGMENTS

T. Cohen-Karni would like to thank the National Science Foundation (CBET1552833) and the Office of Naval Research (N000141712368). The authors would also like to thank Carnegie Mellon University Nanofabrication Facility, and the Department of Materials Science and Engineering Materials Characterization Facility (MCF).

CONFLICT OF INTEREST

Sahil K. Rastogi, Jacqueline Bliley, Daniel J. Shiwarski, Guruprasad Raghavan, Adam W. Feinberg and Tzahi Cohen-Karni declare that they have no conflicts of interest.

ETHICAL APPROVAL

No human studies were carried out by the authors for this article. No animal studies were carried out by the authors for this article.

REFERENCES

[1]Bard, A. J., L. R. Faulkner, J. Leddy, and C. G. Zoski. Electrochemical Methods: Fundamentals and Applications, Vol. 2. New York: Wiley, 1980.
[2]Blake, P., E. Hill, A. Castro Neto, K. Novoselov, D. Jiang, R. Yang, T. Booth, and A. Geim. Making graphene visible. *Appl. Phys. Lett.* 91(6):063124, 2007.
[3]Buckingham, M., S. Meilhac, and S. Zaffran. Building the mammalian heart from two sources of myocardial cells. *Nat. Rev. Genet.* 6(11):826–835, 2005.
[4]Burridge, P. W., E. Matsa, P. Shukla, Z. C. Lin, J. M. Churko, A. D. Ebert, F. Lan, S. Diecke, B. Huber, and N. M. Mordwinkin. Chemically defined generation of human cardiomyocytes. *Nat. Methods* 11(8):855–860, 2014.
[5]Caspi, O., I. Itzhaki, I. Kehat, A. Gepstein, G. Arbel, I. Huber, J. Satin, and L. Gepstein. In vitro electrophysiological drug testing using human embryonic stem cell derived cardiomyocytes. *Stem Cells Dev.* 18(1):161–172, 2009.
[6]Chen, G., D. R. Gulbranson, Z. Hou, J. M. Bolin, V. Ruotti, M. D. Probasco, K. Smuga-Otto, S. E. Howden, N. R. Diol, and N. E. Propson. Chemically defined conditions for human iPSC derivation and culture. *Nat. Methods* 8(5):424–429, 2011.
[7]Clements, M., and N. Thomas. High-throughput multi-parameter profiling of electrophysiological drug effects in human embryonic stem cell derived cardiomyocytes using multi-electrode arrays. *Toxicol. Sci.* 140(2):445–461, 2014.
[8]Cohen-Karni, T., Q. Qing, Q. Li, Y. Fang, and C. M. Lieber. Graphene and nanowire transistors for cellular interfaces and electrical recording. *Nano Lett.* 10(3):1098–1102, 2010.
[9]Deep-Brain Stimulation for Parkinson's Disease Study. Deep-brain stimulation of the subthalamic nucleus or the pars interna of the globus pallidus in Parkinson's disease. *N. Engl. J. Med.* 345(13):956–963, 2001.
[10]Deisseroth, K. Optogenetics. *Nat. Methods* 8(1):26–29, 2011.
[11]Duranteau, J., N. S. Chandel, A. Kulisz, Z. Shao, and P. T. Schumacker. Intracellular signaling by reactive oxygen species during hypoxia in cardiomyocytes. *J. Biol. Chem.* 273(19):11619–11624, 1998.
[12]Epstein, A. E., J. P. DiMarco, K. A. Ellenbogen, N. A. Estes, 3rd, R. A. Freedman, L. S. Gettes, A. M. Gillinov, G. Gregoratos, S. C. Hammill, D. L. Hayes, M. A. Hlatky, L. K. Newby, R. L. Page, M. H. Schoenfeld, M. J. Silka, L. W. Stevenson, M. O. Sweeney, S. C. Smith, Jr, A. K. Jacobs, C. D. Adams, J. L. Anderson, C. E. Buller, M. A. Creager, S. M. Ettinger, D. P. Faxon, J. L. Halperin, L. F. Hiratzka, S. A. Hunt, H. M. Krumholz, F. G. Kushner, B. W. Lytle, R. A. Nishimura, J. P. Ornato, R. L. Page, B. Riegel, L. G. Tarkington, and C. W. Yancy. American College of Cardiology/American Heart Association Task Force on Practice, G.; American Association for Thoracic,

S.; Society of Thoracic, S., ACC/AHA/HRS 2008 Guidelines for Device-Based Therapy of Cardiac Rhythm Abnormalities: a report of the American College of Cardiology/American Heart Association Task Force on Practice Guidelines developed in collaboration with the American Association for Thoracic Surgery and Society of Thoracic Surgeons. *J. Am. Coll. Cardiol.* 51(21):e1–e62, 2008.

[13]Fang, T., A. Konar, H. Xing, and D. Jena. Carrier statistics and quantum capacitance of graphene sheets and ribbons. *Appl. Phys. Lett.* 91(9):092109, 2007.

[14]Feinberg, A. W., C. M. Ripplinger, P. Van Der Meer, S. P. Sheehy, I. Domian, K. R. Chien, and K. K. Parker. Functional differences in engineered myocardium from embryonic stem cell-derived versus neonatal cardiomyocytes. *Stem Cell Rep.* 1(5):387–396, 2013.

[15]Geim, A. K. Graphene: status and prospects. *Science* 324(5934):1530–1534, 2009.

[16]Gross, G. W., W. Y. Wen, and J. W. Lin. Transparent indium-tin oxide electrode patterns for extracellular, multisite recording in neuronal cultures. *J. Neurosci. Methods* 15(3):243–252, 1985.

[17]Hayakawa, T., T. Kunihiro, T. Ando, S. Kobayashi, E. Matsui, H. Yada, Y. Kanda, J. Kurokawa, and T. Furukawa. Image-based evaluation of contraction–relaxation kinetics of human-induced pluripotent stem cell-derived cardiomyocytes: correlation and complementarity with extracellular electrophysiology. *J. Mol. Cell. Cardiol.* 77:178–191, 2014.

[18]Herron, T. J., P. Lee, and J. Jalife. Optical imaging of voltage and calcium in cardiac cells and tissues. *Circ. Res.* 110(4):609–623, 2012.

[19]Huang, S., A. A. Heikal, and W. W. Webb. Two-photon fluorescence spectroscopy and microscopy of NAD (P) H and flavoprotein. *Biophys. J.* 82(5):2811–2825, 2002.

[20]Itzhaki, I., S. Rapoport, I. Huber, I. Mizrahi, L. Zwi-Dantsis, G. Arbel, J. Schiller, and L. Gepstein. Calcium handling in human induced pluripotent stem cell derived cardiomyocytes. *PloS ONE* 6(4):e18037, 2011.

[21]Kasry, A., M. A. Kuroda, G. J. Martyna, G. S. Tulevski, and A. A. Bol. Chemical doping of large-area stacked graphene films for use as transparent, conducting electrodes. *ACS Nano* 4(7):3839–3844, 2010.

[22]Kehat, I., A. Gepstein, A. Spira, J. Itskovitz-Eldor, and L. Gepstein. High-resolution electrophysiological assessment of human embryonic stem cell-derived cardiomyocytes. *Circ. Res.* 91(8):659–661, 2002.

[23]Kehat, I., D. Kenyagin-Karsenti, M. Snir, H. Segev, M. Amit, A. Gepstein, E. Livne, O. Binah, J. Itskovitz-Eldor, and L. Gepstein. Human embryonic stem cells can differentiate into myocytes with structural and functional properties of cardiomyocytes. *J. Clin. Invest.* 108(3):407, 2001.

[24]Kireev, D., S. Seyock, M. Ernst, V. Maybeck, B. Wolfrum, and A. Offenhäusser. Versatile flexible graphene multielectrode arrays. *Biosensors* 7(1):1, 2016.

[25]Kovács, M., J. Tóth, C. Hetényi, A. Málnási-Csizmadia, and J. R. Sellers. Mechanism of blebbistatin inhibition of myosin II. *J. Biol. Chem.* 279(34):35557–35563, 2004.

[26]Kuzum, D., H. Takano, E. Shim, J. C. Reed, H. Juul, A. G. Richardson, J. de Vries, H. Bink, M. A. Dichter, and T. H. Lucas. Transparent and flexible low noise graphene electrodes for simultaneous electrophysiology and neuroimaging. *Nat. Commun.* 5:5259, 2014.

[27]Kwon, J., W. Seung, B. K. Sharma, S.-W. Kim, and J.-H. Ahn. A high performance PZT ribbon-based nanogenerator using graphene transparent electrodes. *Energy Environ. Sci.* 5(10):8970–8975, 2012.

[28]Lee, S., J.-S. Yeo, Y. Ji, C. Cho, D.-Y. Kim, S.-I. Na, B. H. Lee, and T. Lee. Flexible organic solar cells composed of P3HT: PCBM using chemically doped graphene electrodes. *Nanotechnology* 23(34):344013, 2012.

[29]Lian, X., J. Zhang, S. M. Azarin, K. Zhu, L. B. Hazeltine, X. Bao, C. Hsiao, T. J. Kamp, and S. P. Palecek. Directed cardiomyocyte differentiation from human pluripotent stem cells by modulating Wnt/β-catenin signaling under fully defined conditions. *Nat. Protoc.* 8(1):162–175, 2013.

[30]Martin-Puig, S., Z. Wang, and K. R. Chien. Lives of a heart cell: tracing the origins of cardiac progenitors. *Cell Stem Cell* 2(4):320–331, 2008.

[31]Mataev, E., S. K. Rastogi, A. Madhusudan, J. Bone, N. Lamprinakos, Y. Picard, and T. Cohen-Karni. Synthesis of group IV nanowires on graphene: the case of Ge nanocrawlers. *Nano Lett.* 16(8):5267–5272, 2016.

[32]Meyer, T., K.-H. Boven, E. Günther, and M. Fejtl. Microelectrode arrays in cardiac safety pharmacology. *Drug Saf.* 27(11):763–772, 2004.

[33]Mummery, C., D. Ward, C. Van Den Brink, S. Bird, P. Doevendans, T. Opthof, D. La Riviere, A. Brutel, L. Tertoolen, and M. Van Der Heyden. Cardiomyocyte differentiation of mouse and human embryonic stem cells. *J. Anat.* 200(3):233–242, 2002.

[34]Nakahara, M. The Science of Color. Tokyo: Baifukan, 2002.

[35]Novoselov, K. S., A. K. Geim, S. V. Morozov, D. Jiang, Y. Zhang, S. V. Dubonos, I. V. Grigorieva, and A. A. Firsov. Electric field effect in atomically thin carbon films. *Science* 306(5696):666–669, 2004.

[36]Otsuji, T. G., I. Minami, Y. Kurose, K. Yamauchi, M. Tada, and N. Nakatsuji. Progressive maturation in contracting cardiomyocytes derived from human embryonic stem cells: qualitative effects on electrophysiological responses to drugs. *Stem Cell Res.* 4(3):201–213, 2010.

[37]Park, D.-W., A. A. Schendel, S. Mikael, S. K. Brodnick, T. J. Richner, J. P. Ness, M. R. Hayat, F. Atry, S. T. Frye, and R. Pashaie. Graphene-based carbon-layered electrode array technology for neural imaging and optogenetic applications. *Nat. Commun.* 5:6258, 2014.

[38]Pascut, F. C., H. T. Goh, N. Welch, L. D. Buttery, C. Denning, and I. Notingher. Noninvasive detection and imaging of molecular markers in live cardiomyocytes derived from human embryonic stem cells. *Biophys. J.* 100(1):251–259, 2011.

[39]Qiang, Y., K. J. Seo, X. Zhao, P. Artoni, N. H. Golshan, S. Culaclii, P. M. Wang, W. Liu, K. S. Ziemer, and M. Fagiolini. Bilayer nanomesh structures for transparent recording and stimulating microelectrodes. *Adv. Funct. Mater.* 2017. https://doi.org/10.1002/adfm.201704117.

[40]Rastogi, S. K., G. Raghavan, G. Yang, and T. Cohen-Karni. Effect of graphene on nonneuronal and neuronal cell viability and stress. *Nano Lett.* 17(5):3297–3301, 2017.

[41]Saito, R., M. Hofmann, G. Dresselhaus, A. Jorio, and M. Dresselhaus. Raman spectroscopy of graphene and carbon nanotubes. *Adv. Phys.* 60(3):413–550, 2011.

[42]Smith, S. W. The Scientist and Engineer's Guide to Digital Signal Processing. San Diego: California Technical Publishing, 1997.

[43]Spira, M. E., and A. Hai. Multi-electrode array technologies for neuroscience and cardiology. *Nat. Nanotechnol.* 8(2):83–94, 2013.

[44]Stroh, A., H. C. Tsai, L. P. Wang, F. Zhang, J. Kressel, A. Aravanis, N. Santhanam, K. Deisseroth, A. Konnerth, and M. B. Schneider. Tracking stem cell differentiation in the setting of automated optogenetic stimulation. *Stem Cells* 29(1):78–88, 2011.

[45]Suk, J. W., A. Kitt, C. W. Magnuson, Y. Hao, S. Ahmed, J. An, A. K. Swan, B. B. Goldberg, and R. S. Ruoff. Transfer of CVD-grown monolayer graphene onto arbitrary substrates. *ACS Nano* 5(9):6916–6924, 2011.

[46]Thomson, J. A., J. Itskovitz-Eldor, S. S. Shapiro, M. A. Waknitz, J. J. Swiergiel, V. S. Marshall, and J. M. Jones. Embryonic stem cell lines derived from human blastocysts. *Science* 282(5391):1145–1147, 1998.

[47]Tohyama, S., F. Hattori, M. Sano, T. Hishiki, Y. Nagahata, T. Matsuura, H. Hashimoto, T. Suzuki, H. Yamashita, and Y. Satoh. Distinct metabolic flow enables large-scale purification of mouse and human pluripotent stem cell-derived cardiomyocytes. *Cell Stem Cell* 12(1):127–137, 2013.

[48]Wang, G., L. Zhang, and J. Zhang. A review of electrode materials for electrochemical supercapacitors. *Chem. Soc. Rev.* 41(2):797–828, 2012.

[49]Xia, J., F. Chen, J. Li, and N. Tao. Measurement of the quantum capacitance of graphene. *Nat. Nanotechnol.* 4(8):505, 2009.